Complete mapping of the anisotropic free energy of the crystal-melt interface in Al

James R. Morris
Metal and Ceramic Sciences Program, Ames Laboratory (U.S. Department of Energy), Iowa State University, Ames, Iowa 50011
(Received 19 February 2002; revised manuscript received 8 July 2002; published 10 October 2002)

We have calculated the complete anisotropic crystal-melt interfacial free energy of aluminum, using molecular dynamics simulations of the interfaces in equilibrium. The interfacial free energy, $\gamma(\hat{\mathbf{n}})$, can be expressed in terms of two anisotropic parameters, $\epsilon = 1.2\%$ and $\delta = -1.2\%$, as well as an average free energy of $\gamma_0 = 149$ mJ/m^2 in reasonable agreement with current experimental results. The expansion of the free energy in terms of these parameters is consistent with six different orientations, including the (111) interfacial plane, which is found to be rough despite its large stiffness.

DOI: 10.1103/PhysRevB.66.144104 PACS number(s): 68.08.De, 64.70.Dv, 81.10.Aj, 81.05.Bx

I. INTRODUCTION

The study of solidification microstructure has a long history, with interest being driven both by the importance of the microstructure in determining material properties, and by the fundamental interest in the dynamics and pattern formation that occurs.[1–3] Despite many years of effort, fundamental understanding of the dynamics of microstructural development during solidification is still lacking. This is true not only for alloys, but even for the simpler case of pure materials. Without understanding the basic principles that control the dynamics, controlling solidification microstructure remains more of an art than a science.

In the last few years, the importance of anisotropy has been recognized as a necessary factor in determining the form and stability of the interfacial dynamics.[4–6] Both the interfacial free energy and mobilities have important anisotropies that must be determined in order to predict the dynamics. Even a small anisotropy in the free energy on the order of 1% is important, as anisotropy is required for a stable steady-state solution for tip growth in three dimensions. Also, the dynamics of fluctuations, even at very small length scales, play an important role in the ultimate dendritic microstructure.[7] While the importance of this may be understood using phase-field and related continuum models, these approaches neither allow us to evaluate the anisotropies nor to explore the nature of the fluctuations at the atomistic level.

The interfacial free energies for model systems have been calculated for model systems for some time, using a number of techniques: an artificial ''cleaving'' approach, combined with energy integration,[8,9] density functional theory,[10–15] and, most recently, examining the equilibrium fluctuation spectrum of the interface.[16] In the current work, we utilize this last method. We have performed large-scale molecular dynamic (MD) simulations of the solid-liquid interfaces of Al using the embedded-atom method (EAM) with the potential of Ercolessi and Adams.[17] The solid-liquid interfaces are rough, and the magnitude of the fluctuations of the interface depends upon the stiffness of the interface. By examining these fluctuations for various interfaces, we have obtained the interfacial stiffness, which was then used to calculate the interfacial free energy. We describe this approach in the following section. We then describe our simulations in more detail, and present the results from the simulations. These results are discussed in the final section.

II. THEORY AND APPROACH

The approach that we are using to find the interfacial free energy is based upon the fact that for metallic systems, most solid-liquid interfaces of interest will be rough, rather than faceted. For a macroscopically flat interface, we may define the deviation of the height from the average by $\mathrm{h}(\mathbf{x})$, where $\mathbf{x}$ denotes the (two-dimensional) position of the interface. In this work, as we describe below, we treat a discrete description of the heights, h_{ij}, defined on a grid over the cross section of the system, with grid points separated by distances Δ_x and Δ_y. We define the Fourier transform of h_{ij} by

$$h_{\mathbf{q}} = \frac{\Delta_x \Delta_y}{\sqrt{A}} \sum_{ij} h_{ij} \exp(i\mathbf{q}\cdot\mathbf{r}_{ij}), \tag{1}$$

where $\mathbf{r}_{ij} = i\Delta_x\hat{\mathbf{x}} + j\Delta_y\hat{\mathbf{y}}$, and A is the cross-sectional area of the system. With this definition, the height-height correlation function becomes

$$\langle |h_{\mathbf{q}}^2| \rangle = \frac{1}{4} k_B T \left[\frac{\gamma_x}{\Delta_x^2} \sin^2\left(\frac{q_x\Delta_x}{2}\right) + \frac{\gamma_y}{\Delta_y^2} \sin^2\left(\frac{q_y\Delta_y}{2}\right) \right]^{-1}, \tag{2}$$

where γ_x and γ_y are the local stiffness coefficients governing fluctuations in the height in the $\hat{\mathbf{x}}$ and $\hat{\mathbf{y}}$, directions, respectively. In the continuum limit of $q_y = 0$, $q_x\Delta_x \ll 1$, this reduces to

$$\langle |h_{\mathbf{q}}^2| \rangle = \frac{k_B T}{\tilde{\gamma} q^2}, \tag{3}$$

where $\tilde{\gamma}(\hat{\mathbf{n}})$ is the interfacial stiffness for the interface with normal $\hat{\mathbf{n}}$, and $\gamma(\hat{\mathbf{n}})$ is the interfacial free energy as a function of orientation (see, e.g., Ref. 7). These results assume that the height changes slowly as a function of position along the interface. Under these conditions, if the fluctuations of the interface are allowed only about a single angle θ from the nominal orientation $\hat{\mathbf{n}}$, then we may write

$$\tilde{\gamma}(\theta) = \gamma(\theta) + \gamma''(\theta), \tag{4}$$

where the primes indicate differentiation with respect to θ. From this relation, it can be readily shown that the equilibrium fluctuations in the height grow as a function of system size, indicating that these fluctuations are not small deviations from the average height. We note that Eq. (3) differs from that given in Ref. 16 by a factor of the cross-sectional area, presumably due to a different convention for the Fourier transform.

Equation (1) also provides a means for calculating the interfacial stiffness. By simulating the system in equilibrium, we can calculate this correlation function, and thereby derive the interfacial stiffness. Moreover, the stiffness is significantly more anisotropic than the free energy, and therefore its anisotropy is more easily calculated from simulations. For a fourfold symmetry (i.e., rotations about the [100] axis) the simplest form for the interfacial free energy is

$$\gamma(\theta) = \gamma_0(1 + \epsilon_4 \cos 4\theta). \tag{5}$$

In this case, the stiffness is

$$\tilde{\gamma}(\theta) = \gamma_0(1 - 15\,\epsilon_4 \cos 4\theta). \tag{6}$$

This shows that the anisotropy in the interfacial stiffness is larger than that of the free energy by a factor of 15. Where simulations probably could not directly resolve a 1% anisotropy, this larger anisotropy in the stiffness is evident in the simulations, as we demonstrate in this paper.

The full surface $\gamma(\hat{\mathbf{n}})$ can not be specified in the form of Eq. (5), even for weak anisotropy, as it only describes fluctuations about a single angle around a given orientation. Furthermore, while such an expansion may be valid for the interfacial free energy, the interfacial stiffness $\tilde{\gamma}(\hat{\mathbf{n}})$ is considerably more anisotropic, and the expansion in Eq. (4) may not be sufficient as higher-order terms in the anisotropy may be required. These problems have been addressed recently[16] by using "Kubic harmonics"[18] to characterize the interfacial free energy in terms of two anisotropy parameters. The leading terms of the Kubic expansion of the free energy are

$$\gamma(\hat{\mathbf{n}}) = \gamma_0\left[1 - 3\epsilon + 4\epsilon \sum_i n_i^4 + \delta \sum_i n_i^6 - 30\delta n_1^2 n_2^2 n_3^2\right], \tag{7}$$

where we have written the interface normal as $\hat{\mathbf{n}} = (n_1, n_2, n_3)$. For sufficiently small anisotropy, this parametrization of the interfacial free energy in terms of γ_0, ϵ, and δ completely determines the anisotropic free energy for all orientations.

In order to utilize Eq. (3), we must first define a height function derived from atomic configurations. We proceed by defining a local order parameter for each atom, characterizing its environment. For this, we choose a set of N_q wave vectors $\{\mathbf{q}_i\}$ such that

$$\exp(i\mathbf{q}\cdot\mathbf{r}) = 1 \tag{8}$$

for any vector $\mathbf{r}$ connecting near neighbors in a perfect fcc lattice. We omit one of each pair of antiparallel wave vectors; thus, $N_q = 6$. We then define the local order parameter as

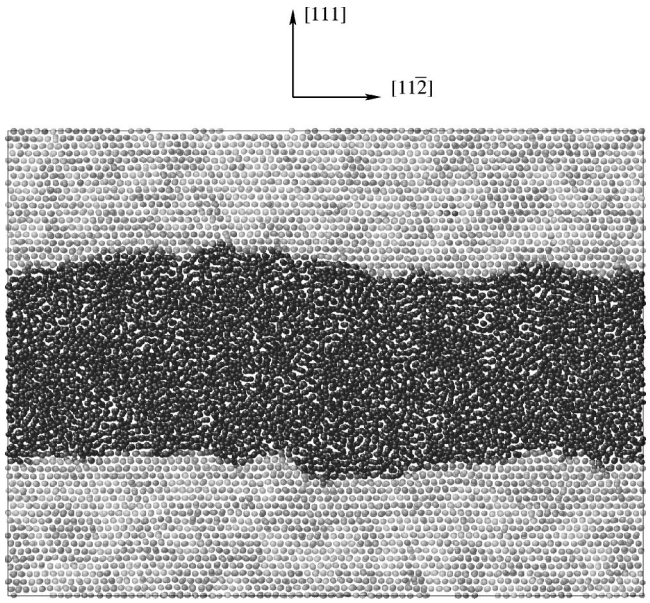

FIG. 1. A snapshot of the system with two (111) interfaces. Atoms have been shaded according to the order parameter defined in Eq. (10), with light atoms having a large value and dark atoms having small values. The order parameter clearly separates the ordered solid region from the disordered, liquid region. The axes on top indicate the crystallographic directions. In the [1$\bar{1}$0] direction (normal to the figure), the periodic repeat distance is significantly shorter than in the other directions.

$$\psi = \left| \frac{1}{N_q} \frac{1}{Z} \sum_{\mathbf{r}} \sum_{\mathbf{q}} \exp(i\mathbf{q}\cdot\mathbf{r}) \right|^2, \tag{9}$$

where the sum on $\mathbf{r}$ runs over each of Z neighbors found within a distance r_c of the atom, chosen to be between the first- and second-neighbor shells in the perfect lattice. This order parameter will equal one for a perfect fcc lattice, and less than one otherwise.

While Eq. (9) is reasonably good at producing an order parameter that is small for the liquid phase and close to one for the solid phase, we have found a couple of methods that improve how well we can discriminate between these phases. First of all, instantaneous atomic positions include significant amounts of fast atomic vibrations that reduce the order of the solid phase. To overcome this, we average the atomic positions over short periods of time ($\sim$50 fs), producing significantly more order in the solid phase. Second, we calculate an *average* order parameter $\bar{\psi}$ for each atom, by averaging over the neighboring values:

$$\bar{\psi}_i = \frac{1}{Z+1}\left(\psi_i + \sum_j \psi_j\right), \tag{10}$$

where j runs over all Z neighbors of atom i. This helps eliminate isolated atoms (or small clusters of atoms) where the local order parameter deviates significantly from its surroundings.

In Fig. 1, we show a snapshot of the system with two (111) interfaces. We have colored the atoms according to their order parameter, as calculated using Eq. (10). As is

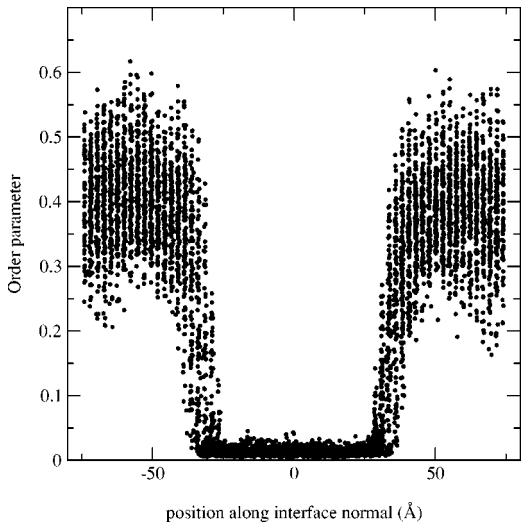

FIG. 2. The order parameter vs position for each atom in an instantaneous configuration of two (111) interfaces (shown in Fig. 1), as a function of atomic position measured along the interface normal. The center region, where the order parameter $\overline{\psi}$ is small, is the liquid region, while the regions where $\overline{\psi}$ is large correspond to the crystal region. The atoms having $0.05 \lesssim \overline{\psi} \lesssim 0.15$ are along the interface.

clear in the figure, we can discriminate between solid and liquid atoms quite well. To make this more quantitative, Fig. 2 shows the values of $\overline{\psi}$ for each atom in a system with coexisting solid and liquid phases, as a function of distance along an axis oriented perpendicular to the interface. As seen in the figure, the liquid region has order parameters with $\overline{\psi} < 0.05$, while the solid region has order parameters with $\overline{\psi} > 0.2$, with an average value of $\langle \overline{\psi} \rangle \approx 0.4$. The two regions are clearly identifiable, and there are very few atoms away from the interface that have values satisfying $0.05 < \overline{\psi} < 0.2$.

This gives a direct method of calculating the average height around a given region: we separate out those atoms that have a value of $\overline{\psi}$ that is distinct from either the solid or liquid ranges, and define those as ''interface'' atoms. The positions of those atoms are then used to define the height h_{ij} of the interface at discrete positions, separated by distances Δ_x and Δ_y in the $\hat{\mathbf{x}}$ and $\hat{\mathbf{y}}$ directions. We have chosen $\Delta_x, \Delta_y \approx a_0$ in order to get good spatial resolution while also ensuring that there are sufficient interfacial atoms to define the height function. Clearly, attempting to define the height function at a resolution finer than typical neighbor distances is artificial. We demonstrate this approach using the configuration shown in Fig. 1. In Fig. 3, the atoms satisfying $0.05 < \overline{\psi} < 0.1$ have been plotted as open circles. These atoms have been separated into bins along the x axis (along the $[11\overline{2}]$ axis), and their positions averaged. The resulting height functions for each interface have been plotted as dark lines. Clearly, we have been able to map out the interface height accurately.

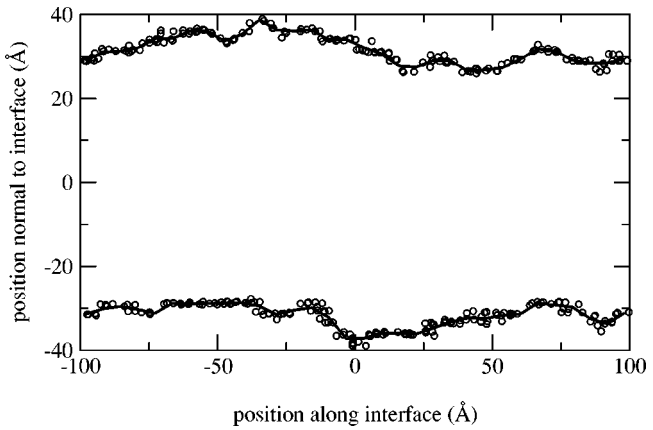

FIG. 3. A demonstration of the calculation of the interface height. The open circles represent the atoms from Fig. 1 whose order parameters satisfy $0.05 < \overline{\psi} < 0.10$. They are clearly localized to the interface. The solid line shows the corresponding height function found using these atomic positions.

An alternate approach to identifying the interface is to characterize each atom by its potential energy. The solid region is clearly then lower in energy than the liquid region. In practice, we found that there was significantly more variation within one phase than with the above order parameter, even with time averaging over short time periods. As a result, it was more difficult to identify the interfacial height using this approach.

III. SIMULATIONS AND INTERFACIAL STIFFNESS CALCULATIONS

We have performed molecular dynamics simulations using the Adams and Ercolessi aluminum potential.[17] This potential has been widely used, and was developed by explicitly fitting the energy and forces in liquid configurations. It has a melting temperature close to the actual melting temperature of $T_m = 933$ K; in our simulations, the average temperature was approximately $T_m = 910$ K.

We chose a simulation that is periodic in all directions, creating two solid-liquid interfaces. We chose our simulations to have a short repeat distance along either the [001] direction (repeat distance of $4a_0$) or the $[1\overline{1}0]$ direction (repeat distance of $2\sqrt{2}a_0$), and a long unit cell in the remaining direction. The geometries are summarized in Table I. The choice of a quasi-two-dimensional geometry, shown for the (100) interface in Fig. 1, enhances fluctuations in the interface, making the analysis easier. Furthermore, Eq. (3) only applies in the long-wavelength limit (compared with interatomic spacings), and this geometry allows us to examine this limit while minimizing the system size. We demonstrate that the results do not depend on the repeat distance thickness at the end of this section.

For these geometries, we can express the stiffness from Eq. (4) in terms of the parameters of the Kubic harmonic expansion in Eq. (7). For the interfaces with a short direction

TABLE I. Summary of interfaces simulated, including the short direction for the simulation, the number of atoms, and the periodic cell geometry (with the *x* direction taken to be the long direction in the interface, the *y* direction to be normal to the interface, and the *z* direction along the short direction). We also provide the expression for the stiffness for each interface derived from Eq. (7), and the interfacial stiffness found from fitting the fluctuation spectrum according to Eq. (3). In parentheses, the value of the stiffnesses calculated using Eq. (7) with our values of γ_0, ϵ, and δ are given.

Interface	Short direction	Number of atoms	System geometry (Å)	Stiffness	$\tilde{\gamma}$ (mJ/m^2)
(100)	[001]	32 768	261.09×138.91×16.32	$\gamma_0(1-15\epsilon-5\delta)$	131 (131)
(110)	[001]	49 152	369.23×148.34×16.32	$\gamma_0(1+15\epsilon+\frac{25}{4}\delta)$	172 (165)
(210)	[001]	40 960	291.94×153.15×16.32	$\gamma_0(1+\frac{21}{5}\epsilon+\frac{11}{5}\delta)$	153 (153)
(110)	$[1\bar{1}0]$	24 576	129.61×297.70×11.49	$\gamma_0(1-9\epsilon+\frac{55}{4}\delta)$	110 (108)
(111)	$[1\bar{1}0]$	19 200	202.56×148.27×11.54	$\gamma_0(1+9\epsilon-\frac{85}{9}\delta)$	174 (182)
(112)	$[1\bar{1}0]$	19 200	143.29×208.66×11.61	$\gamma_0(1+7\epsilon+\frac{205}{36}\delta)$	151 (151)

of [001], we take the angle θ to be the angle between the interface normal and the [100] direction. In this case, the stiffness is

$$\tilde{\gamma}(\theta)/\gamma_0 = 1-3\epsilon-12\epsilon(\cos^4\theta-8\cos^2\theta\sin^2\theta+\sin^4\theta) - 5\delta(\cos^6\theta-6\cos^4\theta\sin^2\theta - 6\sin^4\theta\cos^2\theta+\sin^6\theta). \quad (11)$$

For the geometries where the short direction is $[1\bar{1}0]$, the angle is taken between the interface normal and the [110] direction. The corresponding expression for the stiffness is

$$\tilde{\gamma}(\theta)/\gamma_0 = 1-3\epsilon+6\epsilon(12\cos^2\theta\sin^2\theta-\cos^4\theta-2\sin^4\theta) + \frac{5}{4}\delta(11\cos^6\theta-120\cos^4\theta\sin^2\theta + 96\sin^4\theta\cos^2\theta-4\sin^6\theta). \quad (12)$$

The specific expression for the stiffness for each geometry is listed in Table I.

Our simulations extend for 2×10^6 time steps beyond the equilibration stage (500 000 time steps), with each time step being 0.53 fs. The system naturally evolves toward the equilibrium melting temperature.[19,20] In our simulations, we are integrating Newton's equations, and therefore conserve the total energy. If the temperature (calculated from the kinetic energy) is above the melting temperature, then some of the solid region will melt. This process converts thermal energy to potential energy, through the latent heat of melting. By lowering the thermal energy, the temperature drops towards the melting temperature. Similarly, if the temperature is below the melting temperature, the solid region grows, and the temperature rises towards the melting temperature. As indicated earlier, the average equilibrium temperature in these simulations was close to the real melting point of aluminum. As noted earlier, the average temperature in the simulations was $T_m=910$ K, somewhat lower than the value of $T_m=939\pm5$ K given in Ref. 17. This is due to the fact that during the simulations, the pressure also equilibrates. Our average pressure was $P=-2.5$ kbar; the negative pressure has the effect of lowering the melting temperature (by favoring the less dense liquid phase).

The geometries and numbers of atoms for each interface are given in Table I. During the simulation, we store the atomic positions every 500 time steps, and use these configurations for calculating the height-height correlation function. For each atom, we calculate an order parameter as defined in Eq. (10).

The results for the height-height correlation function are shown in Fig. 4. Error bars indicate the root-mean-square fluctuations of the values. Included in Fig. 4 is a fit to the form given in Eq. (3) for each of the different orientations. Each fit produces a value of $\tilde{\gamma}(\theta)$, where θ is taken to be around the "short" direction of the simulation. In Table I we list the short direction, as well as the expression for the stiffness in terms of the Kubic harmonic expansion given in Eq. (7). The values for the stiffnesses given in Table I, found from the fitting, are not extremely accurate; we estimate errors on the order of 10%. As can be seen in this figure, the results are consistent with a $1/q^2$ dependence, except perhaps at the smallest value of q (longest wavelength). We believe that this deviation for large wavelengths is due to the long equilibration and sampling time associated with the long-wavelength modes. These are precisely the modes whose fluctuations will extend over the longest times, and whose average values will take the longest time to converge. If we continue the simulations significantly longer, these data should also agree with the trend. Even for these modes, our fits are generally within the error bars shown (which are quite large for the smallest values of q). At larger q, there is a suppression of the fluctuations below the $1/q^2$ behavior, which depends on the details of how the height function is calculated. This behavior only occurs at wavelengths approaching that of the lattice constant, where the continuum description [which leads to Eq. (3)] breaks down.

The $1/q^2$ behavior demonstrates that all of the interfaces were indeed rough. This confirms expectations obtained from a visual inspection of instantaneous configurations such as those shown in Fig. 1. The interfaces are not confined to a single atomic layer, although local regions lying close to one layer could often be observed. Such alignments were transient, however, and are eventually destroyed by fluctuations. The case shown in the figure is an extreme case: the (111) interfaces lie along close-packed planes, and could be expected to be faceted instead of rough. Our results given be-

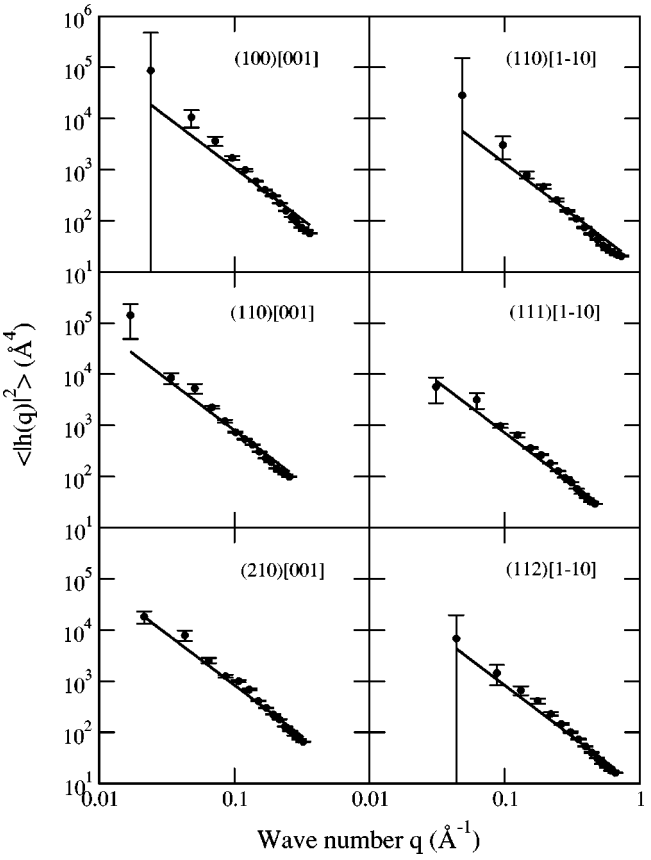

FIG. 4. Power spectrum of the height function, for different interfaces. The interfaces are specified both by the crystallography of the interface, as well as the ''short'' direction of the simulation (either $[001]$ or $[1\bar{1}0]$). Note that Ref. 16 uses the ''long'' direction in their notation instead of the convention used here. The error bars (calculated using the rms deviation of the value) are shown only for the (110) interface. Fits to the form given in Eq. (3) are also shown.

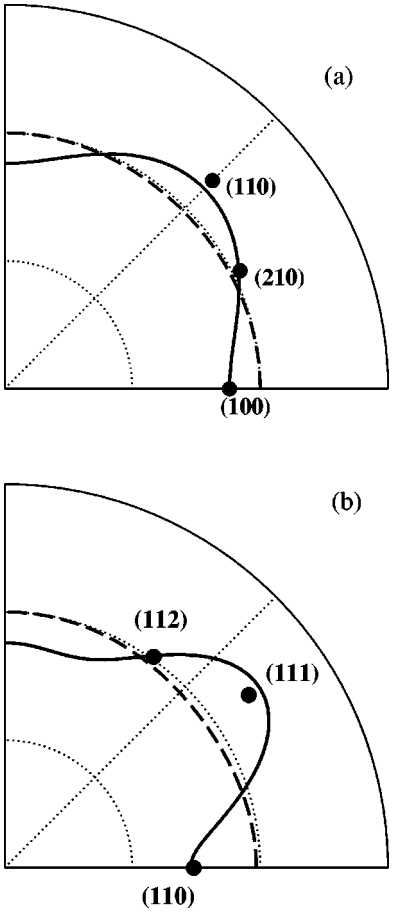

FIG. 5. Interfacial stiffness (solid line) and interfacial free energy (dashed line) vs orientation, for interfaces with normals in (a) the (001) plane and (b) the $(1\bar{1}0)$ plane. In (a), the orientation is characterized by the rotation angle about the [001] direction, with the (100) interface defining $\theta=0$. For (b), the (110) interface defines $\theta=0$. Points indicate the values of the stiffness $\tilde{\gamma}$ found from the height fluctuations. The dotted line lying close to the free energy curve is the contour defined by $\gamma(\hat{\mathbf{n}})=\gamma_0$.

low confirm that the stiffness of this interface is the highest of all of the considered geometries. However, the $1/q^2$ behavior of this interface is clearly shown in Fig. 4.

In Table I, we give the expressions for the stiffnesses for each interface, derived from Eqs. (11) and (12). From these expressions, plus the stiffnesses calculated from the fluctuation spectrum, we found the parameters γ_0, ϵ, and δ by least squares optimization. This gives results of $\gamma_0=149$ mJ/m^2, $\epsilon=1.2\%$, and $\delta=-1.2\%$. We estimate errors in these numbers to be of order 5%. These numbers are in good agreement with grain boundary groove measurements[21] that give a solid Al, liquid Al-Cu interfacial free energy of 163 ± 21 mJ/m^2, and also with the expected low anisotropy of Al. The stiffnesses for all orientations calculated using these parameters are given in parentheses in Table I; as can be seen, the results are very consistent with the fits, with no deviation greater than 5% and usually significantly less. This is smaller than our estimate of the accuracy of these numbers.

In Fig. 5, we show the anisotropic stiffness and free energy as a function of orientation, in both the (100) and (110) plane using these parameters and Eqs. (7), (11), and (12). The data points for the stiffness from the fitting of the height fluctuation spectrum are also shown. As is made clear in this figure, the most significant deviations of the simulation results from the forms given in Eqs. (11) and (12) are where the stiffness is at a local maximum as a function of θ, and therefore where the fluctuations are likely to be the smallest and therefore most difficult to determine. Overall, the data points appear to be very consistent with the forms derived from the Kubic expansion.

Recent experiments[22] have recently determined a value of the anisotropy parameter ϵ_4, defined in Eq. (5), of 0.98%. Note that this parameter is different than the parameter ϵ defined in Eq. (7). We obtain a value of this parameter using the equation for the stiffness given in Eq. (6), and the stiffness data for the (100), (110), and (210) interfaces. In Fig. 6, we plot the stiffness values for these interfaces as a function of $\cos(\theta)$. Linear regression then gives the values $\gamma_0=150$ ± 2 mJ/m^2 and $\epsilon_4=0.009\pm 0.001$. The value of γ_0 is consis-

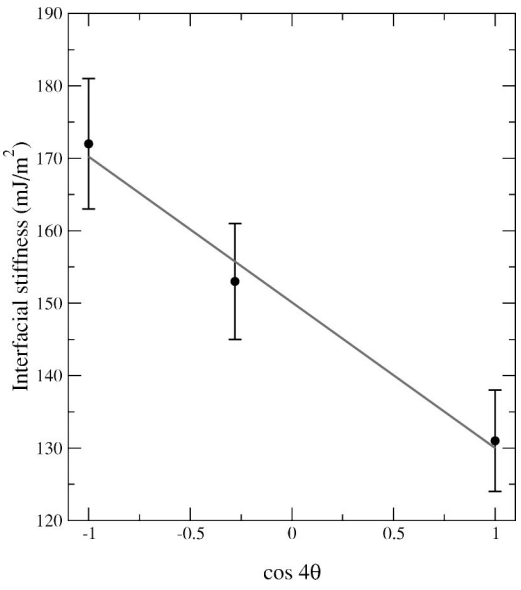

FIG. 6. Stiffness for interfaces perpendicular to the [001] direction, as a function of $\cos 4\theta$. The error bars assume an error of 5%. The linear fit is to the form given in Eq. (6), producing values of $\gamma_0 = 150 \pm 2$ mJ/m^2 and $\epsilon_4 = 0.009 \pm 0.001$.

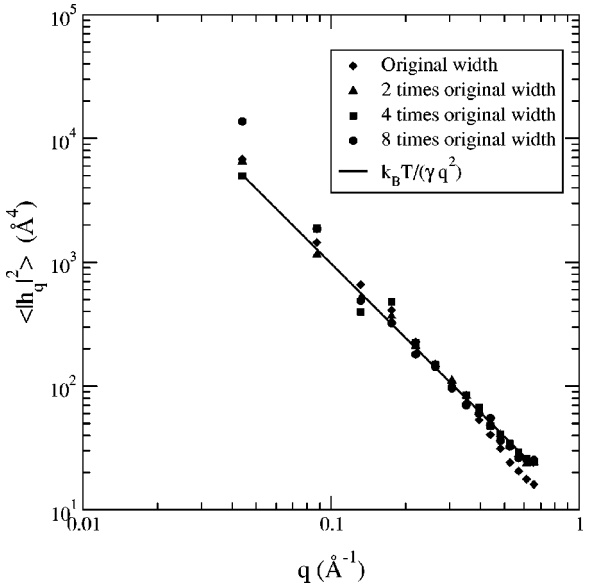

FIG. 7. Height-height correlation functions for the (112) interface, with varying cell sizes along the $[1\bar{1}0]$ direction. Results for the original size (diamonds) are compared with those from systems whose size in the $[1\bar{1}0]$ direction have been multiplied by factors of 2 (triangles), 4 (squares), and 8 (circles). All results are consistent with the data shown in Fig. 4, including the fit to the stiffness value.

tent with our results above, while the value of ϵ_4 is about 10% lower than the experimental value, which is within the error bars of our calculation.

All of the previous simulations use a geometry that has one ''short'' repeat direction. It is not immediately clear that this choice does not limit the possible fluctuations in the system, and thereby affect the results. We have chosen to examine the effects of the system size by explicitly calculating the fluctuations for differently sized systems. We have specifically chosen the $(112)[1\bar{1}0]$ system, and calculated the fluctuations with simulation cells kept fixed in the $\hat{\mathbf{x}}$ and $\hat{\mathbf{z}}$ directions, while multiplying the repeat distance in the $\hat{\mathbf{y}}$ direction by factors of 2, 4, and 8. The results are shown in Fig. 7. As can be seen in the figure, the results are consistent, independent of the system size within the scatter of the data.

IV. DISCUSSION

We have presented a calculation of the full anisotropic crystal-melt interfacial free energy for Al. Similar work has been performed[16] for Ni. These calculations represent the first attempts to evaluate these quantities directly from simulations for real materials. As they are based upon equilibrium properties, they minimize the common problem of the short time scales available to molecular dynamic simulations. One issue in comparing the results to those of real materials is the accuracy of the empirical potential used in the simulations. While the potential used here[17] is widely recognized as being quite reliable for most purposes, it is certainly not completely accurate. We believe that anisotropies that result from these calculations are reasonable.

The calculations rely on the form of the expansion of the free energy in terms of the Kubic harmonics, given in Eq. (7). We calculated the interfacial stiffness for six different interfaces and orientations, which overdetermines the parameters γ_0, ϵ, and δ appearing in this expansion. Our values for these parameters provide a good comparison with all of our results, justifying the use of this expansion.

In order to compare our value of $\gamma_0 = 149$ mJ/m^2 with experiment, we note that there have been repeated discussions[23–26] indicating that the interfacial free energy is proportional to the latent heat L. We write this as

$$\gamma = C_T L \rho^{-1/3}, \tag{13}$$

where the Turnbull coefficient C_T was originally estimated[23,24] to be 0.45 for metals. For aluminum, Turnbull found a value of $\gamma = 93$ mJ/m^2 using nucleation experiments, somewhat lower than our value. However, these experiments[1,24] found that this value was low compared with what is expected from Eq. (13). We find, for the values of the density and latent heat for the aluminum potential used here, $\gamma_0 = 0.58 L \rho^{-1/3}$, which is somewhat higher than the trend that Turnbull observed, but in good agreement with more recent estimates[25,26] of this coefficient. We finally note that our value is close to the value of 163 ± 21 mJ/m^2 found from grain boundary groove measurements for Al in liquid Al-Cu (Ref. 21) and to the value of 160 mJ/m^2 given by Kurz and Fisher.[27]

Another quantity of interest includes the mobilities of the solid-liquid interfaces. These quantities can be examined in a manner similar to the approaches presented here. Just as the height-height correlation function depends upon the interfacial stiffness, the time-dependent fluctuations of the height function are related to the mobility of the interface.[7] Other

approaches, similar in spirit, have been suggested,[28,29] and we are currently examining these approaches.

Finally, we note that all of these calculations are a necessary test before going to the more complicated case of alloy systems. Clearly, the applications of these approaches lie in this area: an approach that allowed us to calculate how alloying elements affect the anisotropic interfacial properties would permit accurate continuum level modeling. This would bridge the gap between the ångstrom/picosecond time scale available to molecular dynamic simulations, and the continuum level modeling that reaches experimental time and length scales. Such calculations would allow much more understanding of the alloy effects, and would permit a more systematic exploration of alloy compositions for real applications.

ACKNOWLEDGMENTS

J.R.M. would like to thank Kai-Ming Ho, Alain Karma, Ralph Napolitano, Xueyu Song, Rohit Trivedi, and Cai-Zhuang Wang for useful input and discussions. This work was funded in part by a Department of Energy Computational Materials Science Network on ''Microstructural Evolution Based on Fundamental Interfacial Properties.'' Computer time was provided by the Scalable Computer Laboratory, Ames Laboratory, and by a grant from NERSC. This research was sponsored by the Division of Materials Sciences and Engineering, Office of Basic Energy Sciences, U.S. Department of Energy, under Contract No. W-7405-ENG-82 with Iowa State University.

[1] D.P. Woodruff, *The Solid-Liquid Interface* (Cambridge University Press, London, 1973).
[2] J.S. Langer, in *Les Houches, Session XLVI, 1986—Chance and Matter*, edited by J. Souletie, R. Stora, and J. Vannimenus (Elsevier Science Publishers, North-Holland, Amsterdam, 1987), p. 629.
[3] J.P. Gollub and J.S. Langer, Rev. Mod. Phys. **71**, S396 (1999).
[4] M. BenAmar and E. Brener, Phys. Rev. Lett. **71**, 589 (1993).
[5] E. Brener, Phys. Rev. Lett. **71**, 3653 (1993).
[6] P. Kopczynski, W.J. Rappel, and A. Karma, Phys. Rev. Lett. **77**, 3387 (1996).
[7] A. Karma, Phys. Rev. E **48**, 3441 (1993).
[8] J.Q. Broughton and G.H. Gilmer, J. Chem. Phys. **84**, 5749 (1986).
[9] R.L. Davidchack and B.B. Laird, Phys. Rev. Lett. **85**, 4751 (2000).
[10] W.A. Curtin, Phys. Rev. Lett. **59**, 1228 (1987).
[11] W.A. Curtin, Phys. Rev. B **39**, 6775 (1989).
[12] D.W. Marr and A.P. Gast, Phys. Rev. E **47**, 1212 (1993).
[13] R. Ohnesorge, H. Lowen, and H. Wagner, Phys. Rev. E **50**, 1994 (1994).
[14] A.D.J. Haymet and D.W. Oxtoby, J. Chem. Phys. **74**, 2559 (1981).
[15] D.W. Oxtoby and A.D.J. Haymet, J. Chem. Phys. **76**, 6262 (1982).
[16] J.J. Hoyt, M. Asta, and A. Karma, Phys. Rev. Lett. **86**, 5530 (2001).
[17] F. Ercolessi and J.B. Adams, Europhys. Lett. **26**, 583 (1994).
[18] A.L. Altman and A.P. Cracknell, Rev. Mod. Phys. **37**, 19 (1965).
[19] J.R. Morris, C.Z. Wang, K.M. Ho, and C.T. Chan, Phys. Rev. B **49**, 3109 (1994).
[20] J.R. Morris and X. Song, J. Chem. Phys. **116**, 9352 (2002).
[21] M. Gündüz and J.D. Hunt, Acta Metall. **33**, 1651 (1985).
[22] S. Liu, R.E. Napolitano, and R. Trivedi, Acta Mater. **49**, 4271 (2001).
[23] D. Turnbull, J. Appl. Phys. **21**, 1022 (1950).
[24] D. Turnbull and R.E. Cech, J. Appl. Phys. **21**, 804 (1950).
[25] Q. Jiang, H.X. Shi, and M. Zhao, Acta Mater. **47**, 2109 (1999).
[26] B.B. Laird, J. Chem. Phys. **115**, 2887 (2001).
[27] W. Kurz and D.J. Fisher, *Fundamentals of Solidification*, 4th ed. (Trans Tech Publications, Uetikon-Zurich, Switzerland, 1998).
[28] W.J. Briels and H.L. Tepper, Phys. Rev. Lett. **79**, 5074 (1995).
[29] A. Karma (private communication).